THE JOURNAL OF BIOLOGICAL CHEMISTRY VOL. 286, NO. 18, pp. 16229–16237, May 6, 2011

Polyethylene Glycol (PEG)-induced Mouse Model of Choroidal Neovascularization*

Received for publication, November 19, 2010, and in revised form, March 18, 2011 Published, JBC Papers in Press, March 23, 2011, DOI 10.1074/jbc.M110.204701

Valeriy V. Lyzogubov, Ruslana G. Tytarenko, Juan Liu, Nalini S. Bora, and Puran S. Bora[1]

From the Department of Ophthalmology, Jones Eye Institute, Pat and Willard Walker Eye Research Center, University of Arkansas for Medical Sciences, Little Rock, Arkansas 72205

In this study, we describe a new method for inducing choroidal neovascularization (CNV) in C57BL/6 mice, an animal model of wet age-related macular degeneration (AMD). AMD is a disease that causes central blindness in humans. We injected PEG-8 subretinally in different doses (0.125–2 mg) to induce CNV. After PEG-8 injection, we examined CNV at several time points (days 3–42). We also used Western blotting, immunohistochemistry, and ELISA to examine the complement component C3 split products, C9, VEGF, TGF-β2, and basic FGF. As early as day 1 after treatment, we found that a single subretinal injection of 1 mg of PEG-8 increased the C3 split products and the C9, TGF-β2, and basic FGF levels in the retinal pigment epithelium-choroid tissue. By day 3 after PEG-8 injection, the intraocular activation of the complement system caused induction and progression of CNV, including new vessels penetrating the Bruch's membrane. At day 5 after PEG-8 injection, we observed a fully developed CNV and retinal degeneration. Thus, in this study, we present a new, inexpensive, and accelerated mouse model of CNV that may be useful to study AMD.

Age-related macular degeneration (AMD)[2] is the leading cause of blindness in the world (1, 2). Early human AMD may persist for many years without any significant vision loss (2, 3). Both reduction of vision and blindness develop at advanced stages, especially in wet AMD with choroidal neovascularization (CNV) (2, 3). CNV causes an accumulation of exudates, including blood in the subretinal space or underneath the retinal pigment epithelium (RPE); retinal detachment; massive photoreceptor loss; and dysfunction leading to blindness (2). In the progression of AMD, the transition from the dry form to the development of primarily the wet form is extremely important. Understanding the mechanisms of CNV formation during its initial phases may be very beneficial in designing new AMD therapeutic strategies for treatment, especially during its early stages (1–3). For this purpose, animal models are very useful to understand human AMD. Currently, there is not an ideal animal model to study human AMD. However, to induce CNV, investigators have used laser photocoagulation, subretinal injections of causative factors, surgical debridement of RPE cells or mechanical rupture of the Bruch's membrane, and transgenic or knock-out animals (4–7).

The role of the complement activation in human AMD and animal AMD models is well accepted in the literature (2, 6, 8–11). One of the central events of the complement activation leading to CNV formation is the deposition of the membrane attack complex (MAC) on the RPE and choroidal cells (8–10, 12, 13). MAC activates synthesis and secretion of VEGF, a major growth factor responsible for CNV growth (8, 12). MAC may cause the death of cells (13, 14), but sublytic concentrations of MAC may activate cell proliferation and migration, modulate cell functions, and induce inflammation (14, 15). We and others support the hypothesis that activation of the complement system and deposition of MAC in the RPE-choroid may lead to CNV development by the increased release or synthesis of growth factors (3, 6, 8–13).

The aim of this study was to create a simple and effective CNV animal model based on the principles of intraocular complement activation. We used a subretinal injection of PEG-8 to induce CNV. PEG is known to activate the complement system (16, 17). Activation of the complement system by an alternative pathway is critical in CNV induction and progression. Phospholipid/methoxy-PEG conjugate is an activator of both the classical and alternative pathways of the complement system (17). A very small amount of PEG is widely used in cosmetic production and drug delivery (18–20). Small molecular weight PEGs are quickly absorbed and excreted. The majority of the administered PEG-8 is eliminated within the first 24 h, and PEG-8 is not metabolized *in vivo* (20). To date, there have not been any studies of the role of PEG in activation of the eye complement system to induce neovascularization or angiogenesis. In this work, we described an angiogenic effect of subretinal PEG administration, investigated the initial events of CNV development, and explored the role of activation of the complement system by PEG in CNV formation.

EXPERIMENTAL PROCEDURES

Animals—Male C57BL/6 mice (7–9 weeks old) were purchased from The Jackson Laboratory (Bar Harbor, ME). This study was approved by the Institutional Animal Care and Use Committee of the University of Arkansas for Medical Sciences.

Subretinal Injection of PEG-8—Subretinal injections were administered as described in the literature (10, 21). The mouse eye was decompressed with a 27-gauge needle by inserting the needle through the conjunctiva and sclera 1 mm behind the

* This work was supported in part by grants from the University of Arkansas for Medical Sciences and the Pat and Willard Walker Eye Research Center.

[1] To whom correspondence should be addressed: Dept. of Ophthalmology, Jones Eye Institute, Pat and Willard Walker Eye Research Center, University of Arkansas for Medical Sciences, 4301 West Markham St., Slot 523-7, Little Rock, AR 72205. Tel.: 501-686-8293; Fax: 501-686-8316; E-mail: pbora@uams.edu.

[2] The abbreviations used are: AMD, age-related macular degeneration; CNV, choroidal neovascularization; RPE, retinal pigment epithelium; MAC, membrane attack complex; CVF, cobra venom factor; bFGF, basic FGF.

limbus. A UMP3 microinjection pump equipped with a Nanofil syringe (100 μl) and a 33-gauge blunt needle (Word Precision Instruments, Sarasota, FL) was used for injections. Needle movement was stopped when light resistance was felt by the operator. An injection of 2 μl of solutions was then administered in 10 s. To investigate the dose-dependent effect of PEG-8 (PEG with a mean M_r of 400; Spectrum Chemicals & Laboratory Products, Gardena, CA), we divided the animals into seven groups. Group 1 (control; n = three mice) was not treated. Group 2 (n = three mice) received a single subretinal injection of the vehicle (2 μl of sterile PBS, Sigma). Groups 3–7 (experimental) were injected with different doses of PEG-8: 2.0, 1.0, 0.5, 0.25, and 0.125 mg. PEG-8 was dissolved in the vehicle before injection, and the volume of all injections used in this study was 2 μl. We applied only a single injection in each experiment. The subretinal injections resulted in some retinal detachment. To determine the optimal dose of PEG-8, we performed a histological examination and a CNV size evaluation at days 5 and 14 after subretinal injection. After the optimal dose was determined, the animals were subretinally injected with 1.0 mg of PEG-8, and three mice from each group were killed at days 1, 3, 4, 5, 7, 14, 21, 28, and 42 post-injection. An evaluation of the CNV size was performed as described below. These experiments were repeated three times.

CNV Size Evaluation—The CNV size was measured as described previously (8–10, 22). The animals from the experimental groups were killed and perfused with 0.75 ml of PBS containing 50 mg/ml FITC-dextran (average M_r of 2,000,000; Sigma). For three-dimensional reconstruction of CNV sites, we captured the Z-stack images of flat mounts (1-μm thick optical slice). We applied a projection tool to build an X-view of these Z-stacks. In addition, we identified the subretinal tissue containing CNV between two layers of cytokeratin 18-positive (RPE) cells.

Histological Investigation and Immunohistochemical Studies—Histological studies of mouse eyes were performed according to Lyzogubov *et al.* (10). Subretinal injections of PEG-8 and PBS were administered to the mice. The animals were killed at days 1, 3, and 5 post-injection (n = five mice, each time point). One set of eyes (n = six eyes from each group) were harvested and fixed with neutral buffered formalin (Sigma). Two eyes from each group were embedded in a composite paraffin block. Serial 5-μm sections were cut. The sections were stained with hematoxylin and eosin and also were used for immunohistochemical staining. Another set of eyes (n = four eyes from each group) were fixed with 2.5% glutaraldehyde prepared on 0.05 M cacodylate buffer, post-fixed with 1% osmium tetroxide, and embedded in Epon 812 resin. All reagents were purchased from Polysciences, Inc. (Warrington, PA). Semithin sections (1 μm) were cut and stained with epoxy tissue stain (Electron Microscopy Sciences, Hatfield, PA). We also used goat anti-C3 polyclonal antibody (Calbiochem), rabbit anti-C9 neoepitope polyclonal antibody (provided by Prof. B. P. Morgan, University of Wales College of Medicine, Cardiff, UK), and goat anti-VEGF polyclonal antibody (R&D Systems, Minneapolis, MN). Anti-C9 antibody recognizes neoepitopes on activated C9 and on C9 in a MAC complex (8–10). To identify the RPE cells, we used mouse anti-cytokeratin 18 monoclonal IgG_1 (Affinity BioReagents, Golden, CO) and Alexa Fluor 594-conjugated phallotoxin (Invitrogen). To identify endothelial cells, we also used rabbit anti-von Willebrand factor polyclonal antibody (Affinity BioReagents) and Alexa Fluor 594-conjugated isolectin IB4 (Invitrogen). The secondary antibodies used were Alexa Fluor 594-conjugated goat anti-mouse IgG (H+L) and Alexa Fluor 488-conjugated donkey anti-rabbit IgG (H+L) (both from Molecular Probes, Eugene, OR) and FITC-conjugated rabbit anti-goat antibody (Zymed Laboratories Inc., South San Francisco, CA). To investigate co-localization of C9 and C3 in the RPE and choroid, we used several paraffin sections. Single-stained sections for C3 (green fluorescence) or C9 (red fluorescence) were used as a control for double-stained (C3 and C9) sections. We performed control staining with isotype-matched control antibodies at concentrations identical to those of the primary antibodies and staining by omission of the primary or secondary antibodies. To block autofluorescence, samples were treated with 1% Sudan Black B (Fisher) as described previously (10).

Microscopy and Image Analysis—We used a Zeiss LSM 510 laser scanning confocal microscope to visualize immunohistochemical staining. To investigate the possible leakage of red and green fluorescence, we captured images of the controls (single-stained sections) using both red and green channels.

For semiquantitative evaluation of C9 deposition in the area of CNV, RPE and choroid sections from each eye were stained for C9, and three images were captured using a Zeiss LSM 510 laser scanning confocal microscope. The integrated intensity of red fluorescence (C9-positive) was measured using NIH ImageJ. We examined slides of the hematoxylin/eosin-stained paraffin sections under an Olympus microscope.

Western Blot Analysis—The complement component C3 split products and C9 in the RPE-choroid were studied as described previously (10). After subretinal injections of PEG-8 and PBS, the animals were killed at days 1, 3, and 5 post-injection (n = five mice, each time point). We extracted the total protein from the pooled RPE-choroid tissue. The following antibodies were used: goat anti-C3 polyclonal antibody, rabbit anti-C9 neoepitope polyclonal antibody, and mouse anti-β-actin monoclonal antibody (Sigma). The control blots were reacted with equivalent concentrations of isotype-matched purified IgG. We performed Western blot analysis using an Amersham ECL Plus enhanced chemiluminescence Western blotting detection system according to the manufacturer's recommendations. This experiment was repeated three times with similar results.

Complement Hemolytic Assays—We subretinally injected PEG-8 (n = 15 mice) and PBS (n = 15 mice) as described above. The animals were killed at days 1, 3, and 5 post-injection. A CH50 assay was performed using methods described in the literature (9, 10, 22, 23). The results are expressed as the reciprocal of this dilution in CH50 units/ml of serum. The alternative pathway activity was calculated as follows: % C3 deposition = (mean % particle fluorescence of sample reaction) − (mean % particle fluorescence of background).

Inhibition of the Systemic Complement System by Cobra Venom Factor—Four groups of animals were used (n = five mice/group). Groups 1 and 2 were treated intraperitoneally

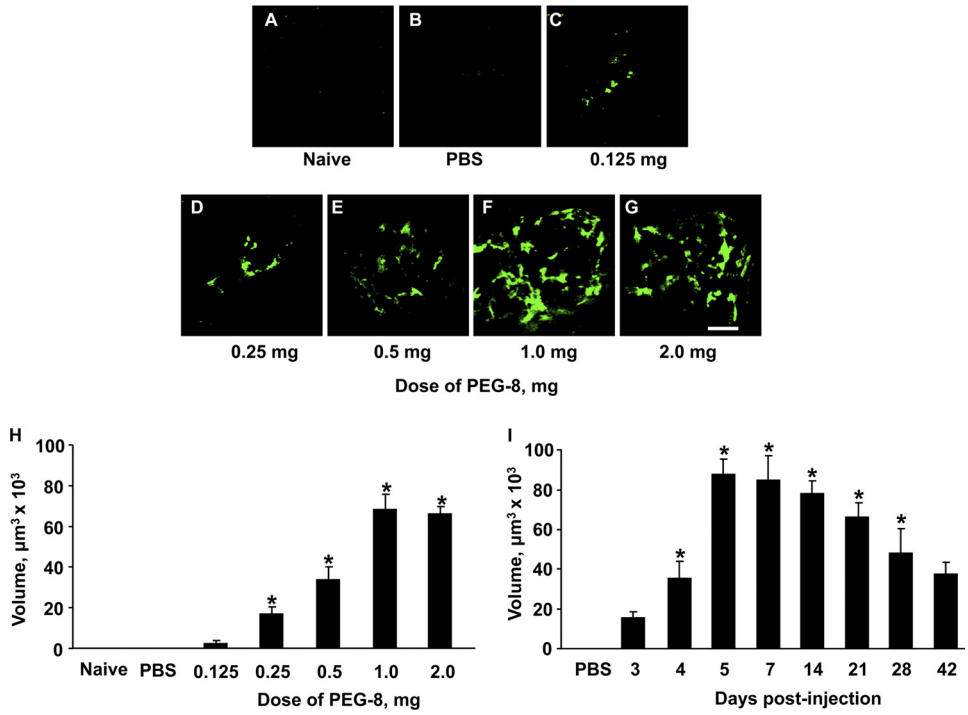

FIGURE 1. **Effect of different doses of PEG-8 on CNV size and time course of PEG-induced CNV.** *A* and *B*, no CNV was found in the naive and PBS-injected animals, respectively. *C–G*, shown is CNV (*green*) after subretinal injections of different doses of PEG-8. *F* and *H*, a PEG-8 dose of 1.0 mg induced CNV of maximal size. *I*, after a subretinal injection of 1 mg of PEG-8, CNV was detected for the first time at day 3 post-injection, was fully developed at day 5, and then started to reduce in size from days 21 to 42. *, $p < 0.05$ *versus* a dose of 0.125 mg (*H*) or day 3 post-injection (*I*). *Scale bar* = 100 μm.

with 4 units of cobra venom factor (CVF; Quidel, San Diego, CA) as described in our previous study (8) for 2 days before and every day after subretinal injections. Groups 3 and 4 were injected intraperitoneally with PBS. Subretinal injections of 1.0 mg of PEG-8 (Groups 1 and 3) or vehicle (Groups 2 and 4) were administered as described above. The animals were killed at day 5 after subretinal injection. Animal serum was collected, and the total complement activity in the serum was measured using the CH50 assay as described above. An evaluation of the CNV size was performed as described above. The RPE-choroid tissues were stained for C9 (neoepitope) using an immunohistochemistry method, and the intensity of the positive signal was analyzed as described above.

ELISA—The animals (n = 15 mice/group) treated with PBS or PEG-8 were killed at days 1, 3, and 5 after subretinal injection. The proteins from the RPE-choroid were prepared as described previously (24, 25) with modifications. The posterior parts of eyes were dissected from enucleated eyes and placed in lysis buffer without detergents. The retina was removed from the RPE-choroid, and the tissue was washed by rotating in ice-cold lysis buffer for 30 s. The tissue was spun down, and the supernatant was collected. This supernatant contained soluble proteins of the extracellular matrix and liquids including exudates of the subretinal space. Lysis buffer with detergents was added to the sediment, and the tissue was homogenized and then treated with a high intensity ultrasonic processor (Sonics & Materials, Inc., Danbury, CT). The tissue was spun down, and the supernatant was collected. This supernatant contained intracellular and membrane-bound proteins. Samples of both extracellular and intracellular fractions of proteins were assayed (in triplicate) for VEGF proteins using mouse VEGF ELISA kits, for TGF-β2 proteins using human TGF-β2 immunoassay, and for basic FGF (bFGF) proteins using human bFGF immunoassay. (All kits were purchased from R&D Systems.) The antibodies against human TGF-β2 and bFGF have very high cross-reactivity with mouse TGF-β2 and bFGF (8). These experiments were repeated three times with similar results.

Statistical Analysis—All of the averaged results are presented as the mean ± S.E. Data were analyzed and compared using the Mann-Whitney test or analysis of variance, and differences were considered statistically significant at $p < 0.05$.

RESULTS

Dose-dependent Effect of PEG-8—We found CNV of different sizes in all PEG-injected groups (Fig. 1, *C–G*). However, CNV was rare and very small (single vessels) in the 0.125 mg-injected group; CNV was larger in the 0.25 mg-injected group compared with the 0.125 mg-injected group. Also, CNV was larger in the 0.5 mg-injected group compared with the 0.25 mg-injected group. The higher doses of 1.0 mg (Fig. 1, *F* and *H*) and 2.0 mg (Fig. 1, *G* and *H*) induced larger and more developed CNV. Thus, we observed a dose-dependent increase in CNV in these animals. We did not observe any CNV in the naive animals (Fig. 1*A*) or in the animals injected with the same volume of sterile PBS (Fig. 1*B*). A dose of 1.0 mg of PEG-8 was selected for the rest of the experiments because it was the minimal dose that resulted in the largest size of CNV.

Time Course of CNV after PEG Injection—C57BL/6 mice were subretinally injected with 1.0 mg of PEG-8 or PBS and killed at days 3, 5, 4, 7, 14, 21, 28, and 42 post-injection. CNV was detected at day 3 after PEG treatment (Fig. 1*I*). CNV reached its largest size at day 5 and was present at least until day

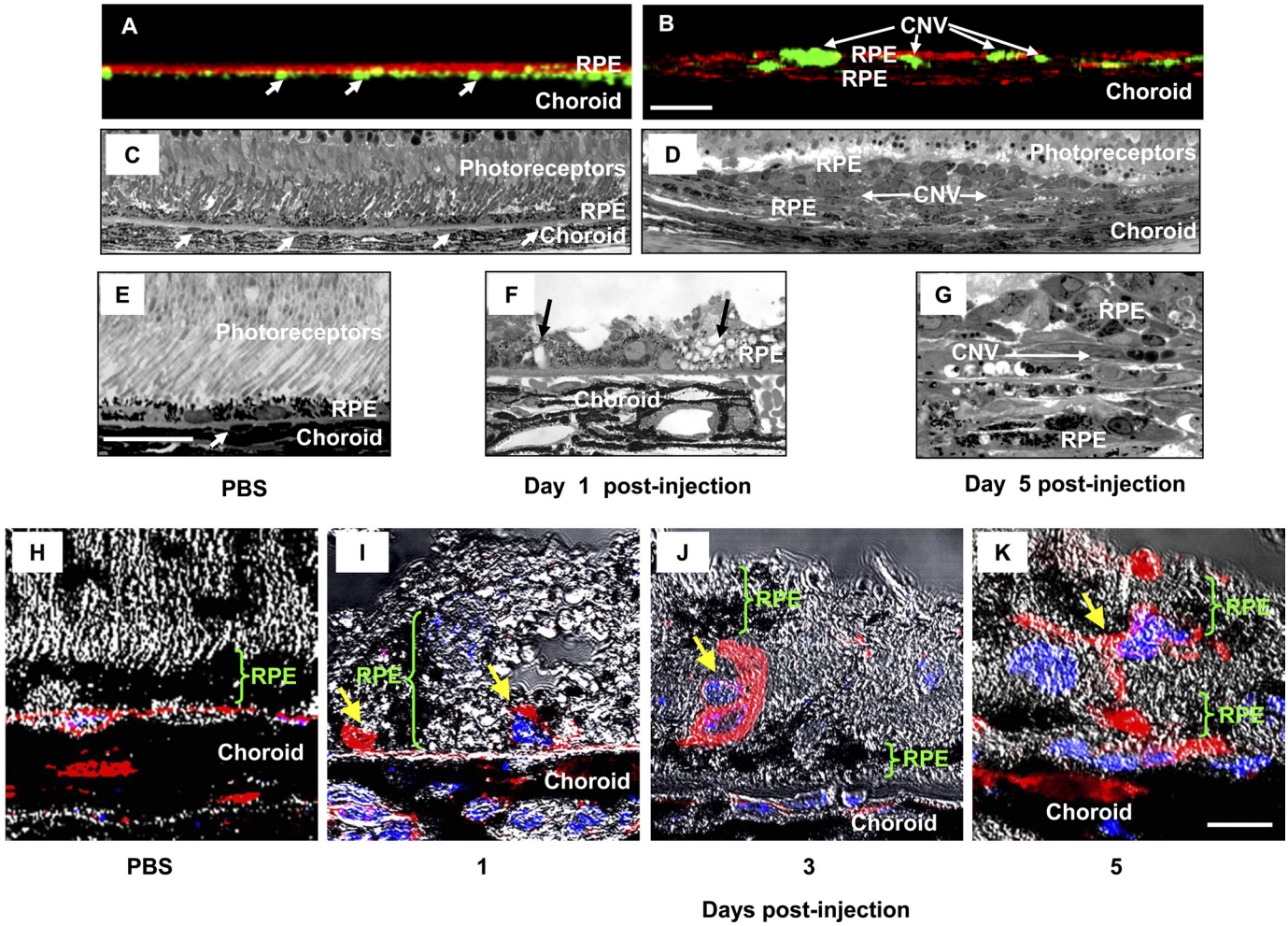

FIGURE 2. **Histological investigation of pathological changes after PEG-8 injection.** *A* and *B*, X-view of the three-dimensional reconstruction of the RPE-choroid flat mounts of PBS- and PEG-8-treated animals, respectively. FITC-dextran-perfused vessels (*arrow*) are *green*, and the RPE cells stained with cytokeratin 18 are *red*. Subretinal tissue, including CNV, is located between two layers of the RPE cells (existing and newly growing). *C–E* and *G*, microphotographs of Epon-embedded semithin eye sections (1 μm) of PBS-injected mice (*C* and *E*) and PEG-8-injected mice (*D* and *G*) killed at day 5 post-injection. Subretinal tissue and CNV are located between two layers of the RPE cells, vessels containing erythrocytes marked with *arrows*. *F*, microphotograph of a semithin eye section of PEG-8-injected mice killed at day 1 post-injection showing the increased size of the RPE cells and vacuoles in the RPE cells (*arrows*). *H–K*, microphotographs of 5-μm paraffin sections of PBS-injected mice (*H*) and PEG-8-injected mice killed at day 1 (*I*), 3 (*J*), and 5 (*K*) post-injection. Isolectin IB4-labeled (*red*) endothelial cells penetrated the Bruch's membrane and growth between the RPE cells (*I*); endothelial cells proliferated in the subretinal space and formed new vessels partially covered by a new layer of RPE cells (*J* and *K*). The nuclei of cells were stained with DAPI (*blue*). *Scale bars* = 50 μm (*A–D*), 20 μm (*E–G*), and 10 μm (*H–K*).

42 after injection. The CNV size was almost the same at days 7 and 14 but started decreasing from days 21 to 42. We did not detect any CNV in the PBS-injected animals (Fig. 1*I*).

Localization of PEG-8-induced CNV—In PBS-treated animals, FITC-dextran-perfused vessels were present under cytokeratin 18-positive RPE cells within the choroid (Fig. 2*A*). CNV in the PEG-8-injected animals was localized between two layers of cytokeratin 18-positive RPE cells (Fig. 2*B*). Investigation of the semithin Epon-embedded sections (1 μm) showed that the RPE formed a single cell layer and that the choroidal vessels were located exclusively within the choroid (Fig. 2, *C* and *E*). In PEG-8-injected mice at day 1 after injection, we found an increased size of the RPE cells and the vacuolization of the RPE cell cytoplasm (Fig. 2*F*) compared with the controls. At day 5 after PEG-8 injection, we found CNV located between two layers of the RPE cells in the subretinal space (Fig. 2, *D* and *G*). None of the vessels that originated from the retina were found in this area (Fig. 2*D*). We investigated the immunohistochemical staining by the endothelial cell marker isolectin IB4 in 5-μm paraffin sections of PBS- and PEG-8-injected mice at days 1, 3, and 5 after treatment. The RPE cells in the PBS-treated group formed a single layer of cells, and endothelial cells were found within the choroid (Fig. 2*H*). Beginning with day 1 after PEG-8 treatment, we found isolectin IB4-positive endothelial cells between the cells (Fig. 2*I*). These cells penetrated the Bruch's membrane, invaded the space between the RPE cells, and had contact with existing choroidal capillaries. At day 3 after injection, new vessels were formed from these cells in the subretinal space, and a second layer of RPE cells was also formed (Fig. 2*J*). The newly developed vessels, located in the subretinal space, formed a CNV complex at day 5 after PEG-8 injection (Fig. 2*K*).

Retinal Changes after PEG-8 Injection—At day 5 after PEG-8 or PBS injection, we performed a histological investigation of the paraffin sections of the mouse eyes. We observed a reduced thickness of the outer nuclear layer and photoreceptor outer

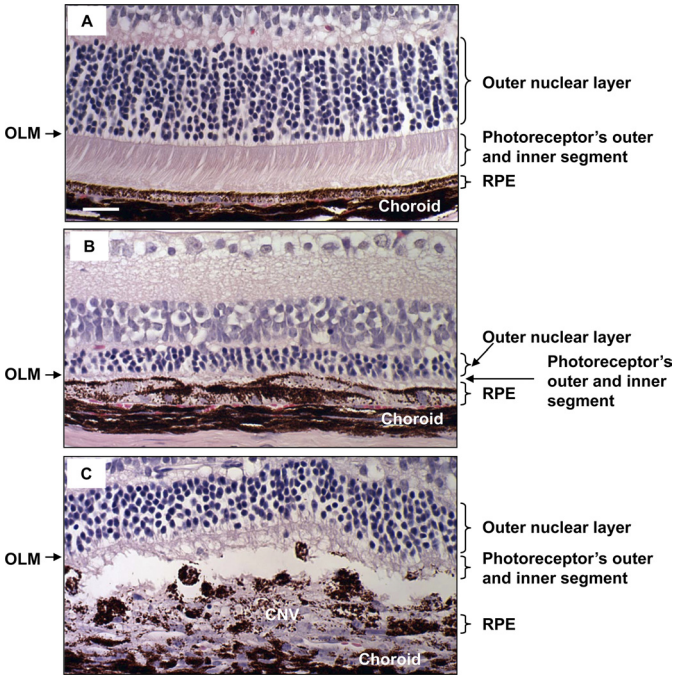

FIGURE 3. **Retinal changes after PEG-8 injection.** Shown are microphotographs of paraffin sections of PBS-injected (*A*) and PEG-8-injected (*B* and *C*) animals killed at day 5 post-injection stained with hematoxylin and eosin. A decreased thickness of the outer nuclear layer and photoreceptor inner and outer segments was found in PEG-8-treated animals (*B* and *C*) compared with PBS-treated controls (*A*). *OLM*, outer limiting membrane. *Scale bar* = 20 μm.

and inner segments in PEG-8-treated animals compared with PBS-injected controls (Fig. 3).

PEG-8-induced CNV by Complement System Activation—The total complement activity in the sera of the CVF-treated mice (Fig. 4*A*) was significantly reduced compared that in the PBS-injected animals. We found areas of high C9 deposition in the PBS-treated (complement-sufficient) animals (Fig. 4*B*) but not in the CVF-treated (complement-depleted) group (Fig. 4*C*). C9-positive fluorescence in PBS-treated animals was significantly higher compared with that in CVF-injected mice (Fig. 4*H*). Analysis of the CNV size showed that treatment with CVF significantly (5-fold) reduced the volume of FITC-dextran-perfused vessels (Fig. 4, *E* and *I*) compared with PBS-injected animals (Fig. 4, *D* and *I*). We did not observe any staining in the negative controls (Fig. 4, *F* and *G*).

Activation of the Complement System by PEG-8 in the RPE-Choroid—PEG-8 did not affect the total and alternative complement activities in mouse serum at all time points investigated (Fig. 5, *A* and *B*). However, we found an increase in the levels of the C3 split products (43 and 23 kDa) in the PEG-8-injected animals compared with the PBS-injected mice at day 1 post-injection (Fig. 5, *C–E*) in the RPE-choroid tissue. Interestingly, in the RPE-choroid tissue at days 3 and 5, the levels of the 43-kDa C3 split product were higher in the PEG-8-treated animals compared with the PBS-injected mice (Fig. 5, *C* and *D*), but the levels of the 23-kDa C3 split product were reduced in the PEG-8-treated animals compared with the PBS-injected mice (Fig. 5, *C* and *E*). Western blot analysis showed that the C9

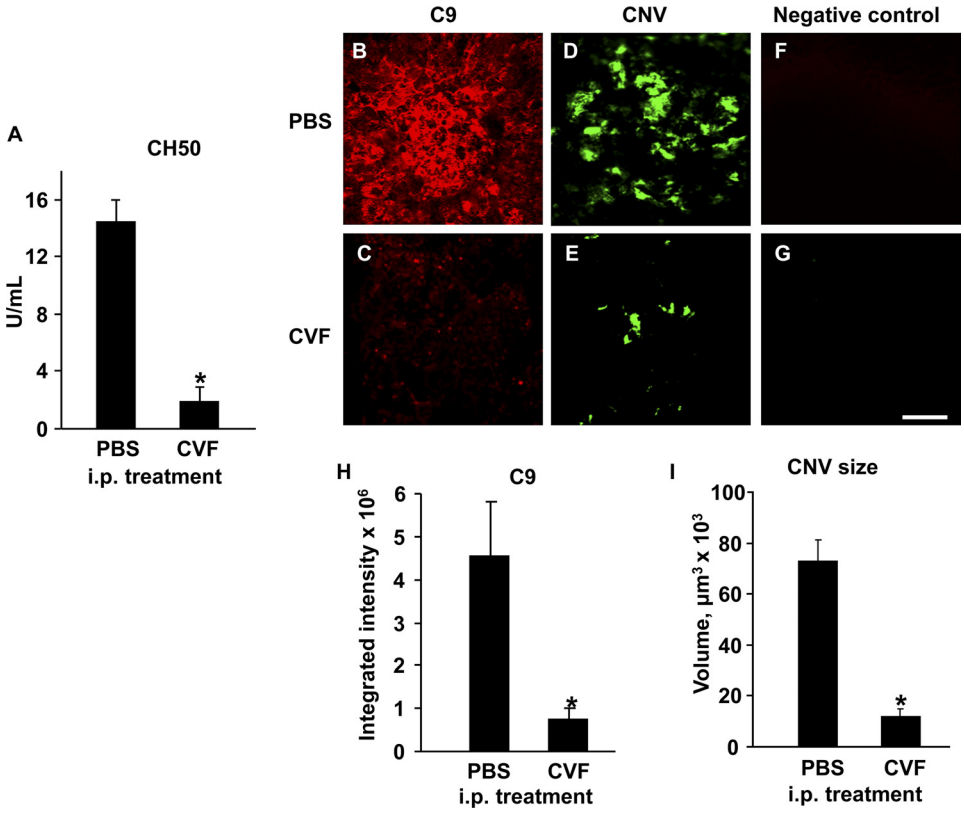

FIGURE 4. **Effect of complement depletion with CVF on PEG-8-induced C9 deposition and CNV size.** Intraperitoneal treatment with CVF significantly reduced total complement activity in mouse serum compared with PBS-treated animals (*A*). C9 deposition (*red*; *B*, *C*, and *H*) and CNV size (*D*, *E*, and *I*) were significantly reduced in CVF-treated animals. Negative controls with no primary antibodies are also shown (*F* and *G*). *, $p < 0.05$ compared with the PBS-treated group. *i.p.*, intraperitoneal. *Scale bar* = 100 μm.

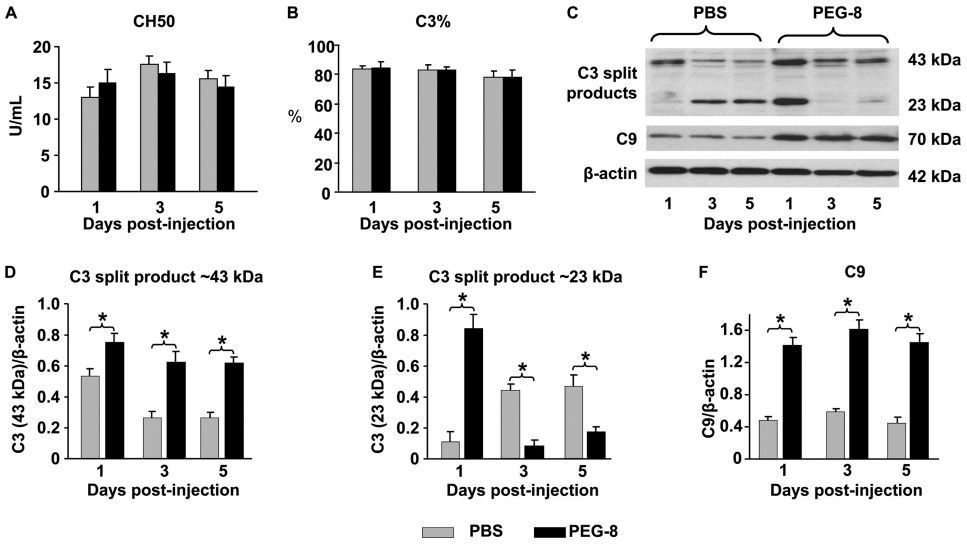

FIGURE 5. **Effect of PEG-8 on complement activity in serum and RPE-choroid.** A subretinal injection of PEG-8 did not affect total (*A*) and alternative (*B*) complement activities in mouse serum at any day post-treatment. Western blot analysis of RPE-choroid tissue showed that PEG-8 increased C3 split products (43 and 23 kDa) at day 1 post-injection (*C–E*) and C9 at all days post-injection (*C* and *F*). *b-actin*, β-actin. *, $p < 0.05$.

levels were ~3-fold higher in the RPE-choroid tissue from the PEG-8-treated mice compared with the PBS-treated animals at all time points investigated (Fig. 5, *C* and *F*).

Relationship between Complement Activation, Growth Factor Expression, and CNV Growth—We performed a co-localization experiment to study the relationship between C3/C9 deposition, VEGF expression, and CNV growth initiation after PEG-8 injection. Staining of the eye sections from control animals showed a co-localization of C9 and C3 in the RPE and choroid (Fig. 6, *A*, *B*, and *D*). At day 1 after PEG-8 injection, C9 was found mostly in the sites of increased C3 deposition (Fig. 6, *H*, *I*, and *K*). C9 was detected not only on the surface but also in the cytoplasm of the RPE cells (Fig. 6, *O* and *Q*). We discovered that the initiation of CNV growth occurred in the sites of very high C9 deposition (Fig. 6, *O–Q*).

In the control animals, VEGF was found in the center of the RPE cells and outlining the apical and basal cellular membranes (Fig. 7, *A–C*). After PEG-8 treatment, we detected an increase in the VEGF-positive staining of the apical side of the RPE and within the choroid (Fig. 7, *D–F*). Choroidal capillaries and the growing endothelial cells were co-localized with VEGF (Fig. 7, *D–F*). We investigated the growth factors VEGF, TGF-β2, and bFGF using ELISA in extracellular (water-soluble) and intracellular (after adding detergent) fractions of proteins obtained from the RPE and choroid of the eyes treated with PBS or PEG-8. We detected high intracellular VEGF levels at day 3 and secreted VEGF at day 5 after PEG-8 injection (Fig. 7, *G* and *H*) compared with the control group. Investigation of TGF-β2 showed a significant increase in the TGF-β2 protein in both intracellular and extracellular fractions at day 1 after PEG-8 injection compared with the PBS-treated animals (Fig. 7, *I* and *J*). Later, at days 3 and 5, we found an increased amount of TGF-β2 in the extracellular fractions of the PEG-8-treated mice compared with the PBS-treated animals (Fig. 7, *I* and *J*). ELISA analysis of bFGF in the RPE-choroid tissue revealed an increased expression of this protein at days 1, 3, and 5 post-injection (intracellular fraction) and an increased secretion of bFGF at days 3 and 5 post-injection (extracellular fraction) (Fig. 7, *K* and *L*).

DISCUSSION

The hallmark of wet AMD is the presence of CNV. The macular region of the retina plays a key role in the central vision of humans. The high dependence of the macula on the choroidal blood supply is the "Achilles' heel" of the human eye. With age and certain risk factors, this unique way of supplying the nutrients to the macula becomes impaired. Uncontrolled choroidal vessel growth can cause severe and usually irreversible changes in the photoreceptor-RPE-choroid interactions (1, 3). Untreated neovascular or wet AMD can cause central blindness in humans and affect their quality of life. Understanding the mechanisms of CNV formation will assist in the development of better treatment strategies for human AMD.

In this study, we have described an economical, simple, and quick experimental CNV mouse model by using a single subretinal injection of PEG-8. The injected PEG-8 spreads between the neuronal retina and the RPE cells and creates a subretinal bleb visible through a dilated pupil under a microscope. The pathological changes observed in this new accelerated mouse model greatly mimic human wet AMD. We detected the early events of CNV formation in existing choroidal capillaries at day 1 after PEG-8 treatment. These initial phases include RPE cell enlargement and vacuolization, formation of sprouts from pre-existing choroidal capillaries, and penetration into the Bruch's membrane in several sites as seen in human wet AMD (1). The formation of new vessels was noted at day 3 after treatment in the subretinal space. By day 5, the CNV complex reached its maximal size and started decreasing from day 21. The early stages of human CNV formation have been poorly investigated by researchers (1). Subclinical CNV, not evidenced by fundus investigation, is a growth of the endothelial cells in combination with the fibrovascular tissue into the sub-RPE or subretinal space through breaks in the Bruch's membrane and is characterized by extensive endothelial cell proliferation and migration

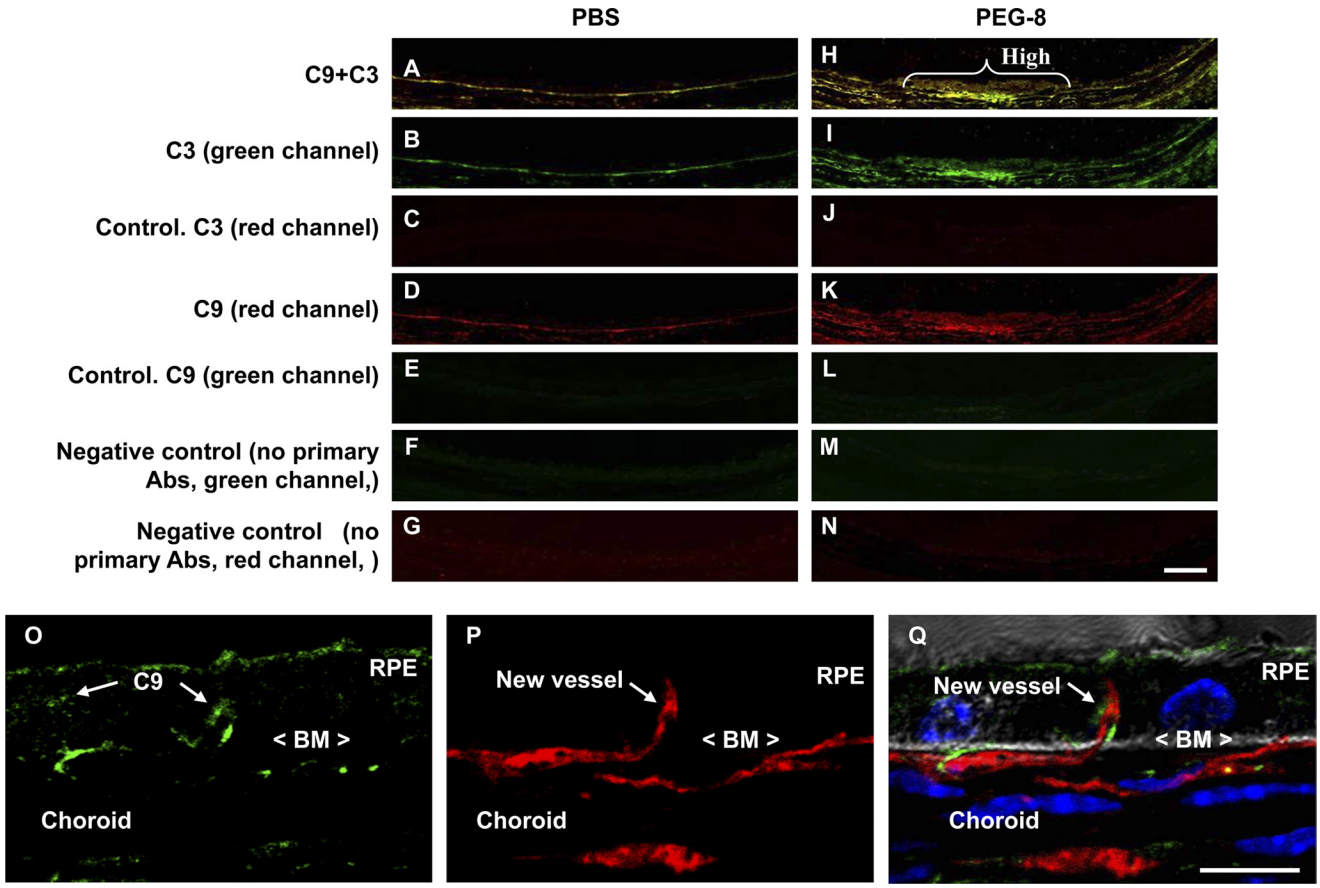

FIGURE 6. **Immunohistochemical staining for C3 and C9 at sites of CNV induction.** Microphotographs of PBS-treated (*A–G*) and PEG-8-treated (*H–N*) animals (confocal microscopy) show co-localization of C3 and C9 (*yellow*; *A* and *H*), C3 (*green*; *B* and *I*), control for C3 captured using a red channel (*red*; *C* and *J*), C9 (*red*; *D* and *K*), control for C9 captured using a red channel (*red*; *E* and *L*), and negative controls (no primary antibodies) for C3 (*green*; *F* and *M*) and C9 (*red*; *G* and *N*). A high deposition of C9 and C3 (*yellow*; *H*, *white brace*) on the RPE and choroid in PEG-8-treated animals was observed at the sites of penetration of the Bruch's membrane (*BM*) by endothelial cells (*O–Q*) at day 1 post-treatment. *Scale bars* = 20 μm (*A–N*) and 50 μm (*O–Q*).

(1, 26). Drusen, RPE degeneration, and hyperpigmentation are the first clinical signs of early AMD (3).

In humans, detection of the early stages of CNV growth is very difficult. The use of animal models is necessary for investigation of the early events leading to CNV initiation and progression. To induce CNV, subretinal injections of different agents have been used. These agents include lipid hydroperoxide in rats, autologous vitreous in rabbits, bFGF-containing microspheres in rabbits, and VEGF-impregnated microspheres in monkeys (4–7, 27). The laser photocoagulation method is commonly used to develop CNV in different species (4–6, 8–10). To achieve CNV induction in the laser-induced animal model, it is necessary for the RPE cells, Bruch's membrane, and choroid to be damaged by a laser. A subretinal injection of PEG-8 produced less damage to the RPE and choroid compared with the laser-induced CNV model. Although a subretinal model of CNV has been described previously in rats by a subretinal injection of Matrigel (28, 29), the PEG-induced model has not been described before.

PEG-8 is well tolerated and known to activate the complement system, especially an alternative pathway (16). We found a dose-dependent effect of PEG-8 on the CNV size. We suggest that increasing the PEG-8 concentration may lead to higher hydration of complement component C3 and activation of the complement system by an alternative pathway. We found that a subretinal injection of PEG-8 induced activation of the complement system at the injection site but not in the blood system. Inhibition of the complement system by CVF significantly reduced C9 deposition in and around the injection sites and also inhibited the CNV size. This supports the idea that activation of the complement system is a necessary event in the induction of CNV (2, 8–11). At day 1 after PEG-8 treatment, we detected complement component C3 deposition and increased levels of the C3 split products in the RPE-choroid tissue. The C3 split products with molecular masses of ~23 and 43 kDa may belong to the α-chain of iC3b or C3c. The presence of C3 split products such as iC3b and C3c is an indicator of an inflammatory state (30). A significant increase in the C3 split products at day 1 after PEG-8 injection confirms activation of the complement system. The reduction of the 23-kDa split product in the PEG-8-treated animals at days 3 and 5 post-injection may reflect an increased destruction of this fragment. At the same time, at day 1 post-injection of PEG-8, we detected an increase in C9 deposition in the eye but not in the systemic circulation. Complement component C3 deposition on the RPE-choroid was co-localized with C9 deposition, followed by morphological changes in the RPE cells and CNV development. We noticed that the increased levels of C9 and the 43-kDa C3 split product in the RPE and choroid were present for a longer duration (day 5).

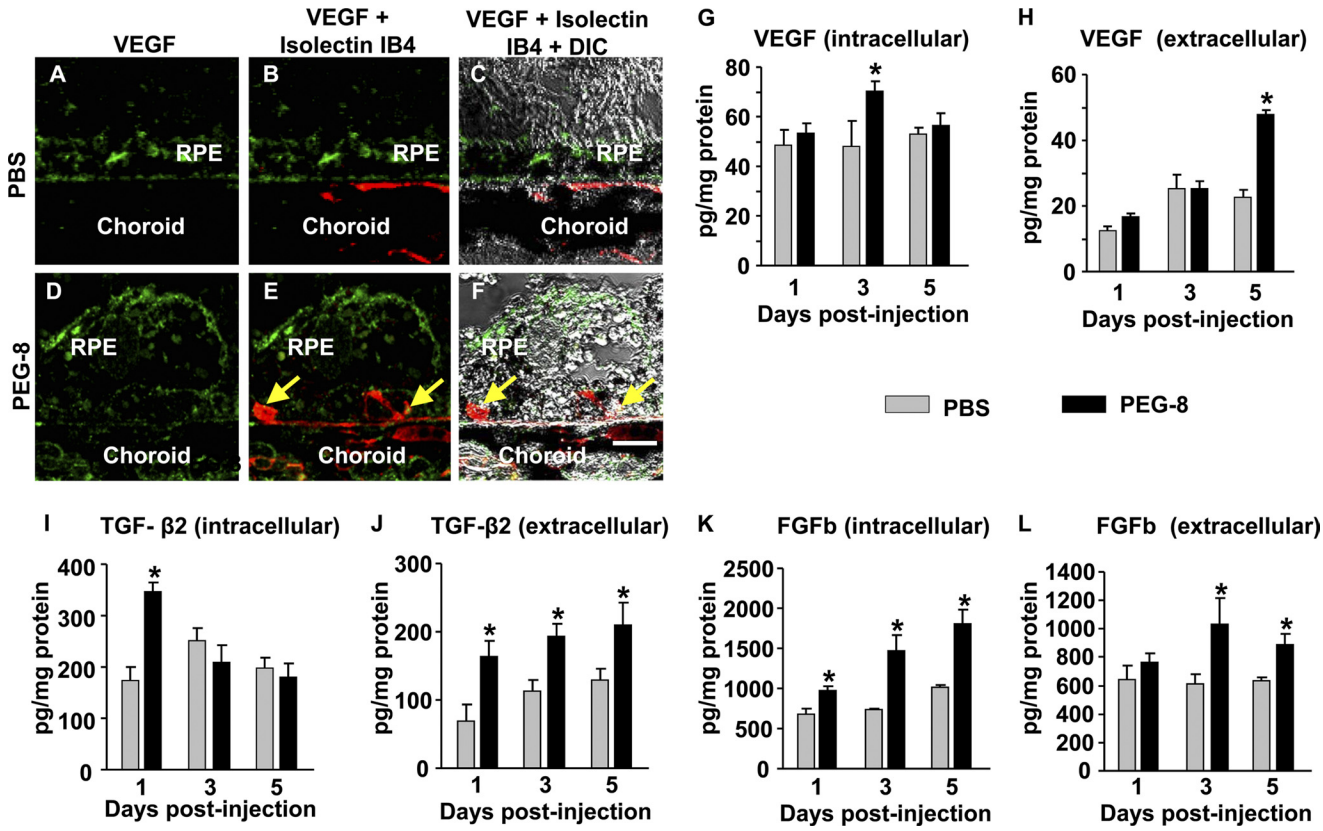

FIGURE 7. **Effect of PEG-8 on VEGF and other growth factors in the RPE-choroid.** Microphotographs of paraffin sections show that PEG-8 increased VEGF expression on the apical side of the RPE and within the choroid (*green*; *D–F*) compared with the PBS-treated control (*A–C*). VEGF ELISA showed significantly increased levels of VEGF in the intracellular fraction of the RPE-choroid at day 3 after PEG treatment (*G*) and significantly increased levels of VEGF in the extracellular fraction of RPE-choroid at day 5 (*H*). TGF-β2 ELISA demonstrated significantly increased levels of TGF-β2 in the intracellular fraction at day 1 after PEG treatment (*I*) and significantly increased levels of TGF-β2 in the extracellular fraction of the RPE-choroid at days 1, 3, and 5 (*J*). bFGF (*FGFb*) ELISA showed significantly increased levels of bFGF in the intracellular fraction of the RPE-choroid at day 1, 3, and 5 after PEG treatment (*K*) and significantly increased levels of bFGF in the extracellular fraction of the RPE-choroid at days 3 and 5 (*L*). *DIC*, differential interference contrast. *, $p < 0.05$ compared with the PBS-treated group. *Scale bar* = 10 μm.

We found that the RPE cells increased in size and became round-shaped in the areas of high C9 deposition. C9 deposition on RPE cells affects cell-cell interactions (13). Also, C9 deposition leads to vesiculation of RPE cells, a rounded shape, loss of normal hexagonal morphology, and loss of defined cell borders (13). We demonstrated in this study that C9 induces the stimulation of RPE and endothelial cells. However, Halperin *et al.* (15) have shown that sublytic concentrations of MAC can stimulate cell proliferation. Complement system activation and MAC deposition may induce production and release of growth factors (8, 12). VEGF, TGF-β2, and bFGF are known as important growth factors for neovascularization in humans and experimental animals (1, 3, 8, 9). Under normal conditions, RPE cells secrete VEGF to their basal and apical sides to maintain the homeostasis of the photoreceptor-RPE-Bruch's membrane-choroid microenvironment (31–34). In this study, we found that VEGF was mostly in the RPE cells of the control animals. However, a very small amount of VEGF was found in the choroid. This is a typical localization of VEGF in the RPE and choroid as described in humans and experimental animals (1, 3). In AMD, the RPE expresses high levels of VEGF and promotes CNV (3). We detected increased expression and secretion of VEGF after PEG-8 treatment. We also detected growth of endothelial cells penetrating the Bruch's membrane and entering the subretinal space. We observed an increased synthesis and a secretion of TGF-β2 and bFGF after a subretinal injection of PEG-8. Interestingly, this increased secretion of TGF-β2 (day 1) and bFGF (day 3) preceded an increased secretion of VEGF (day 5) after treatment with PEG-8. C9 deposition stimulated growth factor expression and secretion, followed by RPE and endothelial cell transformation, proliferation, and migration.

In this study, we discovered that an acute and high local complement activation by a PEG-8 injection in the posterior pole of the mouse eye leads to CNV initiation. It is known that mutations in factor H, factor B, and C2 of the complement system not only increase the risk of CNV (wet AMD) but also can increase drusen formation and geographic atrophy (dry AMD) (35–37). Rohrer and co-workers (38) have shown that chronic sublytic activation of the complement system is associated with oxidative RPE damage and increased RPE VEGF production.

The advantages of this experimental model of CNV formation are as follows. 1) Mice are economical and easy to handle; 2) the procedure to induce CNV does not require expensive equipment or reagents; 3) the complement activation by PEG-8 occurs for only a limited time, and CNV formation begins very soon (3 days) after treatment; 4) the primary damage of the RPE-choroid after subretinal injection is much smaller com-

pared with laser treatment or surgical procedures; 5) the pathological changes after PEG-8 injection are limited only to the posterior pole of the mouse eye; and 6) the local (intraocular) stimulation of VEGF expression and secretion by PEG-8 mimics the changes seen in human AMD. It has been noted that regardless of its etiological factors, morphology, and cellular composition, the resulting CNV is remarkably similar to human AMD (7). Despite the differences in the time course of CNV observed in humans and the proposed model, the absence of the macula in mice, and the role of multiple risk factors in the pathogenesis of AMD, this CNV model may be very useful to study CNV formation and to test various inhibitors that prevent neovascular AMD. The angiogenic role of PEG has been described previously in myocardial ischemia (39), but the role of PEG in CNV has not been described before this study. Thus, our study opens up a new area of PEG application not only in generating a new AMD model but also in wound healing, where angiogenesis is needed for quick healing.

Acknowledgments—We thank Cynthia Bond for editing and Dr. P. Jha for critical review of the manuscript.

REFERENCES

1. Campochiaro, P. A. (2000) *J. Cell. Physiol.* **184,** 301–310
2. Coleman, H. R., Chan, C. C., Ferris, F. L., 3rd, and Chew, E. Y. (2008) *Lancet* **372,** 1835–1845
3. Zarbin, M. A. (2004) *Arch. Ophthalmol.* **122,** 598–614
4. Montezuma, S. R., Vavvas, D., and Miller, J. W. (2009) *Semin. Ophthalmol.* **24,** 52–61
5. Elizabeth Rakoczy, P., Yu, M. J., Nusinowitz, S., Chang, B., and Heckenlively, J. R. (2006) *Exp. Eye Res.* **82,** 741–752
6. Edwards, A. O., and Malek, G. (2007) *Angiogenesis* **10,** 119–132
7. Lassota, N. (2008) *Acta Ophthalmol.* **86,** 1–28
8. Bora, P. S., Sohn, J. H., Cruz, J. M., Jha, P., Nishihori, H., Wang, Y., Kaliappan, S., Kaplan, H. J., and Bora, N. S. (2005) *J. Immunol.* **174,** 491–497
9. Bora, N. S., Kaliappan, S., Jha, P., Xu, Q., Sohn, J. H., Dhaulakhandi, D. B., Kaplan, H. J., and Bora, P. S. (2006) *J. Immunol.* **177,** 1872–1878
10. Lyzogubov, V. V., Tytarenko, R. G., Jha, P., Liu, J., Bora, N. S., and Bora, P. S. (2010) *Am. J. Pathol.* **177,** 1870–1880
11. Anderson, D. H., Radeke, M. J., Gallo, N. B., Chapin, E. A., Johnson, P. T., Curletti, C. R., Hancox, L. S., Hu, J., Ebright, J. N., Malek, G., Hauser, M. A., Rickman, C. B., Bok, D., Hageman, G. S., and Johnson, L. V. (2010) *Prog. Retin. Eye Res.* **29,** 95–112
12. Li, W., Chen, S., Ma, M., Qian, J., and Ma, X. (2010) *Med. Sci. Monit.* **16,** BR17–BR23
13. Ramo, K., Cashman, S. M., and Kumar-Singh, R. (2008) *Invest. Ophthalmol. Vis. Sci.* **49,** 4126–4136
14. Morgan, B. P. (1989) *Biochem. J.* **264,** 1–14
15. Halperin, J. A., Taratuska, A., and Nicholson-Weller, A. (1993) *J. Clin. Invest.* **91,** 1974–1978
16. Hamad, I., Hunter, A. C., Szebeni, J., and Moghimi, S. M. (2008) *Mol. Immunol.* **46,** 225–232
17. Moein Moghimi, S., Hamad, I., Bünger, R., Andresen, T. L., Jørgensen, K., Hunter, A. C., Baranji, L., Rosivall, L., and Szebeni, J. (2006) *J. Liposome Res.* **16,** 167–174
18. Veronese, F. M., and Pasut, G. (2005) *Drug Discov. Today* **10,** 1451–1458
19. Yamaoka, T., Tabata, Y., and Ikada, Y. (1995) *J. Pharm. Sci.* **84,** 349–354
20. Final Report on the Safety Assessment of Triethylene Glycol and PEG-4 (2006) *Int. J. Toxicol.* **25,** 121–138
21. Shen, W. Y., and Rakoczy, P. E. (2001) *Antisense Nucleic Acid Drug Dev.* **11,** 257–264
22. Bora, N. S., Jha, P., Lyzogubov, V. V., Kaliappan, S., Liu, J., Tytarenko, R. G., Fraser, D. A., Morgan, B. P., and Bora, P. S. (2010) *J. Biol. Chem.* **285,** 33826–33833
23. Huang, Y., Qiao, F., Atkinson, C., Holers, V. M., and Tomlinson, S. (2008) *J. Immunol.* **181,** 8068–8076
24. Itaya, M., Sakurai, E., Nozaki, M., Yamada, K., Yamasaki, S., Asai, K., and Ogura, Y. (2007) *Invest. Ophthalmol. Vis. Sci.* **48,** 5677–5683
25. Rohrer, B., Long, Q., Coughlin, B., Wilson, R. B., Huang, Y., Qiao, F., Tang, P. H., Kunchithapautham, K., Gilkeson, G. S., and Tomlinson, S. (2009) *Invest. Ophthalmol. Vis. Sci.* **50,** 3056–3064
26. Killingsworth, M. C. (1995) *Graefes Arch. Clin. Exp. Ophthalmol.* **233,** 313–323
27. Baba, T., Bhutto, I. A., Merges, C., Grebe, R., Emmert, D., McLeod, D. S., Armstrong, D., and Lutty, G. A. (2010) *Am. J. Pathol.* **176,** 3085–3097
28. Zhao, L., Wang, Z., Liu, Y., Song, Y., Li, Y., Laties, A. M., and Wen, R. (2007) *Mol. Vis.* **14,** 873–880
29. Cao, J., Zhao, L., Li, Y., Liu, Y., Xiao, W., Song, Y., Luo, L., Huang, D., Yancopoulos, G. D., Wiegand, S. J., and Wen, R. (2010) *Invest. Ophthalmol. Vis. Sci.* **51,** 6009–6017
30. Palarasah, Y., Skjodt, K., Brandt, J., Teisner, B., Koch, C., Vitved, L., and Skjoedt, M. O. (2010) *J. Immunol. Methods* **362,** 142–150
31. Blaauwgeers, H. G., Holtkamp, G. M., Rutten, H., Witmer, A. N., Koolwijk, P., Partanen, T. A., Alitalo, K., Kroon, M. E., Kijlstra, A., van Hinsbergh, V. W., and Schlingemann, R. O. (1999) *Am. J. Pathol.* **155,** 421–428
32. Sonoda, S., Sreekumar, P. G., Kase, S., Spee, C., Ryan, S. J., Kannan, R., and Hinton, D. R. (2010) *Aging* **2,** 28–42
33. Saint-Geniez, M., Kurihara, T., Sekiyama, E., Maldonado, A. E., and D'Amore, P. A. (2009) *Proc. Natl. Acad. Sci. U.S.A.* **106,** 18751–18756
34. Saint-Geniez, M., Maldonado, A. E., and D'Amore, P. A. (2006) *Invest. Ophthalmol. Vis. Sci.* **47,** 3135–3142
35. Haddad, S., Chen, C. A., Santangelo, S. L., and Seddon, J. M. (2006) *Surv. Ophthalmol.* **51,** 316–363
36. Donoso, L. A., Kim, D., Frost, A., Callahan, A., and Hageman, G. (2006) *Surv. Ophthalmol.* **51,** 137–152
37. Klein, R. J., Zeiss, C., Chew, E. Y., Tsai, J. Y., Sackler, R. S., Haynes, C., Henning, A. K., SanGiovanni, J. P., Mane, S. M., Mayne, S. T., Bracken, M. B., Ferris, F. L., Ott, J., Barnstable, C., and Hoh, J. (2005) *Science* **308,** 385–389
38. Thurman, J. M., Renner, B., Kunchithapautham, K., Ferreira, V. P., Pangburn, M. K., Ablonczy, Z., Tomlinson, S., Holers, V. M., and Rohrer, B. (2009) *J. Biol. Chem.* **284,** 16939–16947
39. Pawliuk, R., and Leboulch, P. (November 22, 2001) WIPO Patent Application WO/2001/087312